Properties of Heavy Secondary Fluorine Cosmic Rays: Results from the Alpha Magnetic Spectrometer

Editors' Suggestion

Properties of Heavy Secondary Fluorine Cosmic Rays: Results from the Alpha Magnetic Spectrometer

M. Aguilar,[30] L. Ali Cavasonza,[1] M. S. Allen,[10] B. Alpat,[37] G. Ambrosi,[37] L. Arruda,[28] N. Attig,[24] F. Barao,[28] L. Barrin,[15] A. Bartoloni,[43] S. Başeğmez-du Pree,[18,*] R. Battiston,[40,41] M. Behlmann,[10] B. Beranek,[1] J. Berdugo,[30] B. Bertucci,[37,38] V. Bindi,[20] K. Bollweg,[21] B. Borgia,[43,44] M. J. Boschini,[32] M. Bourquin,[16] E. F. Bueno,[18] J. Burger,[10] W. J. Burger,[40] S. Burmeister,[26] X. D. Cai,[10] M. Capell,[10] J. Casaus,[30] G. Castellini,[14] F. Cervelli,[39] Y. H. Chang,[48,49] G. M. Chen,[6,7] G. R. Chen,[23] H. S. Chen,[6,7] Y. Chen,[16,23] L. Cheng,[23] H. Y. Chou,[49] S. Chouridou,[1] V. Choutko,[10] C. H. Chung,[1] C. Clark,[10,21] G. Coignet,[3] C. Consolandi,[20] A. Contin,[8,9] C. Corti,[20] Z. Cui,[22,23] K. Dadzie,[10] C. Delgado,[30] S. Della Torre,[32] M. B. Demirköz,[2] L. Derome,[17] S. Di Falco,[39] V. Di Felice,[45,†] C. Díaz,[30] F. Dimiccoli,[40] P. von Doetinchem,[20] F. Dong,[35] F. Donnini,[45,†] M. Duranti,[37] A. Egorov,[10] A. Eline,[10] J. Feng,[10] E. Fiandrini,[37,38] P. Fisher,[10] V. Formato,[45,†] C. Freeman,[20] Y. Galaktionov,[10] C. Gámez,[30] R. J. García-López,[27] C. Gargiulo,[15] H. Gast,[1] M. Gervasi,[32,33] F. Giovacchini,[30] D. M. Gómez-Coral,[20] J. Gong,[35] C. Goy,[3] V. Grabski,[31] D. Grandi,[32,33] M. Graziani,[37,38] S. Haino,[48] K. C. Han,[29] R. K. Hashmani,[2] Z. H. He,[19] B. Heber,[26] T. H. Hsieh,[10] J. Y. Hu,[6,7] M. Incagli,[39] W. Y. Jang,[13] Yi Jia,[10] H. Jinchi,[29] K. Kanishev,[40] B. Khiali,[45,†] G. N. Kim,[13] Th. Kirn,[1] M. Konyushikhin,[10] O. Kounina,[10] A. Kounine,[10] V. Koutsenko,[10] A. Kuhlman,[20] A. Kulemzin,[10] G. La Vacca,[32,33] E. Laudi,[15] G. Laurenti,[8] I. Lazzizzera,[40,41] A. Lebedev,[10] H. T. Lee,[47] S. C. Lee,[48] J. Q. Li,[35] M. Li,[1] Q. Li,[35] S. Li,[1] J. H. Li,[22] Z. H. Li,[6,7] J. Liang,[22] C. Light,[20] C. H. Lin,[48] T. Lippert,[24] J. H. Liu,[5] Z. Liu,[16] S. Q. Lu,[48] Y. S. Lu,[6] K. Luebelsmeyer,[1] J. Z. Luo,[35] Xi Luo,[23] S. S. Lyu,[19] F. Machate,[1] C. Mañá,[30] J. Marín,[30] J. Marquardt,[26] T. Martin,[10,21] G. Martínez,[30] N. Masi,[8,9] D. Maurin,[17] A. Menchaca-Rocha,[31] Q. Meng,[35] V. V. Mikhailov,[34] D. C. Mo,[19] M. Molero,[30] P. Mott,[10,21] L. Mussolin,[37,38] J. Negrete,[20] N. Nikonov,[1] F. Nozzoli,[40] A. Oliva,[8] M. Orcinha,[28] M. Palermo,[20] F. Palmonari,[8,9] M. Paniccia,[16] A. Pashnin,[10] M. Pauluzzi,[37,38] S. Pensotti,[32,33] H. D. Phan,[10] R. Piandani,[25] V. Plyaskin,[10] S. Poluianov,[36] X. Qin,[10] Z. Y. Qu,[48] L. Quadrani,[8,9] P. G. Rancoita,[32] D. Rapin,[16] A. Reina Conde,[27] E. Robyn,[16] S. Rosier-Lees,[3] A. Rozhkov,[10] D. Rozza,[32,33] R. Sagdeev,[11] S. Schael,[1] A. Schulz von Dratzig,[1] G. Schwering,[1] E. S. Seo,[12] Z. Shakfa,[2] B. S. Shan,[4] T. Siedenburg,[1] C. Solano,[10] J. W. Song,[22] X. J. Song,[23] R. Sonnabend,[1] L. Strigari,[43,‡] T. Su,[23] Q. Sun,[22] Z. T. Sun,[6,7] M. Tacconi,[32,33] X. W. Tang,[6] Z. C. Tang,[6] J. Tian,[37,38] Samuel C. C. Ting,[10,15] S. M. Ting,[10] N. Tomassetti,[37,38] J. Torsti,[50] C. Tüysüz,[2] T. Urban,[10,21] I. Usoskin,[36] V. Vagelli,[42,37] R. Vainio,[50] M. Valencia-Otero,[49] E. Valente,[43,44] E. Valtonen,[50] M. Vázquez Acosta,[27] M. Vecchi,[18] M. Velasco,[30] J. P. Vialle,[3] C. X. Wang,[22] L. Wang,[5] L. Q. Wang,[22] N. H. Wang,[22] Q. L. Wang,[5] S. Wang,[20] X. Wang,[10] Yu Wang,[22] Z. M. Wang,[23] J. Wei,[16] Z. L. Weng,[10] H. Wu,[35] R. Q. Xiong,[35] W. Xu,[22,23] Q. Yan,[10] Y. Yang,[46] I. I. Yashin,[34] H. Yi,[35] Y. M. Yu,[19] Z. Q. Yu,[6] M. Zannoni,[32,33] C. Zhang,[6] F. Zhang,[6] F. Z. Zhang,[6,7] J. H. Zhang,[35] Z. Zhang,[10] F. Zhao,[6,7] C. Zheng,[23] Z. M. Zheng,[4] H. L. Zhuang,[6] V. Zhukov,[1] A. Zichichi,[8,9] and P. Zuccon[40,41]

(AMS Collaboration)

[1]*I. Physics Institute and JARA-FAME, RWTH Aachen University, 52056 Aachen, Germany*
[2]*Department of Physics, Middle East Technical University (METU), 06800 Ankara, Turkey*
[3]*Université Grenoble Alpes, Université Savoie Mont Blanc, CNRS, LAPP-IN2P3, 74000 Annecy, France*
[4]*Beihang University (BUAA), Beijing, 100191, China*
[5]*Institute of Electrical Engineering (IEE), Chinese Academy of Sciences, Beijing, 100190, China*
[6]*Institute of High Energy Physics (IHEP), Chinese Academy of Sciences, Beijing, 100049, China*
[7]*University of Chinese Academy of Sciences (UCAS), Beijing, 100049, China*
[8]*INFN Sezione di Bologna, 40126 Bologna, Italy*
[9]*Università di Bologna, 40126 Bologna, Italy*
[10]*Massachusetts Institute of Technology (MIT), Cambridge, Massachusetts 02139, USA*
[11]*East-West Center for Space Science, University of Maryland, College Park, Maryland 20742, USA*
[12]*IPST, University of Maryland, College Park, Maryland 20742, USA*
[13]*CHEP, Kyungpook National University, 41566 Daegu, Korea*
[14]*CNR-IROE, 50125 Firenze, Italy*
[15]*European Organization for Nuclear Research (CERN), 1211 Geneva 23, Switzerland*
[16]*DPNC, Université de Genève, 1211 Genève 4, Switzerland*
[17]*Université Grenoble Alpes, CNRS, Grenoble INP, LPSC-IN2P3, 38000 Grenoble, France*
[18]*Kapteyn Astronomical Institute, University of Groningen, P.O. Box 800, 9700 AV Groningen, Netherlands*

[19]Sun Yat-Sen University (SYSU), Guangzhou, 510275, China
[20]Physics and Astronomy Department, University of Hawaii, Honolulu, Hawaii 96822, USA
[21]National Aeronautics and Space Administration Johnson Space Center (JSC), Houston, Texas 77058, USA
[22]Shandong University (SDU), Jinan, Shandong, 250100, China
[23]Shandong Institute of Advanced Technology (SDIAT), Jinan, Shandong, 250100, China
[24]Jülich Supercomputing Centre and JARA-FAME, Research Centre Jülich, 52425 Jülich, Germany
[25]Institut für Experimentelle Teilchenphysik, Karlsruhe Institute of Technology (KIT), 76131 Karlsruhe, Germany
[26]Institut für Experimentelle und Angewandte Physik, Christian-Alberts-Universität zu Kiel, 24118 Kiel, Germany
[27]Instituto de Astrofísica de Canarias (IAC), 38205 La Laguna, and Departamento de Astrofísica, Universidad de La Laguna, 38206 La Laguna, Tenerife, Spain
[28]Laboratório de Instrumentação e Física Experimental de Partículas (LIP), 1649-003 Lisboa, Portugal
[29]National Chung-Shan Institute of Science and Technology (NCSIST), Longtan, Tao Yuan, 32546, Taiwan
[30]Centro de Investigaciones Energéticas, Medioambientales y Tecnológicas (CIEMAT), 28040 Madrid, Spain
[31]Instituto de Física, Universidad Nacional Autónoma de México (UNAM), Ciudad de México, 01000 Mexico
[32]INFN Sezione di Milano-Bicocca, 20126 Milano, Italy
[33]Università di Milano-Bicocca, 20126 Milano, Italy
[34]NRNU MEPhI (Moscow Engineering Physics Institute), Moscow, 115409 Russia
[35]Southeast University (SEU), Nanjing, 210096, China
[36]Sodankylä Geophysical Observatory and Space Physics and Astronomy Research Unit, University of Oulu, 90014 Oulu, Finland
[37]INFN Sezione di Perugia, 06100 Perugia, Italy
[38]Università di Perugia, 06100 Perugia, Italy
[39]INFN Sezione di Pisa, 56100 Pisa, Italy
[40]INFN TIFPA, 38123 Povo, Trento, Italy
[41]Università di Trento, 38123 Povo, Trento, Italy
[42]Agenzia Spaziale Italiana (ASI), 00133 Roma, Italy
[43]INFN Sezione di Roma 1, 00185 Roma, Italy
[44]Università di Roma La Sapienza, 00185 Roma, Italy
[45]INFN Sezione di Roma Tor Vergata, 00133 Roma, Italy
[46]National Cheng Kung University, Tainan, 70101, Taiwan
[47]Academia Sinica Grid Center (ASGC), Nankang, Taipei, 11529, Taiwan
[48]Institute of Physics, Academia Sinica, Nankang, Taipei, 11529, Taiwan
[49]Physics Department and Center for High Energy and High Field Physics, National Central University (NCU), Tao Yuan, 32054, Taiwan
[50]Space Research Laboratory, Department of Physics and Astronomy, University of Turku, 20014 Turku, Finland

(Received 20 December 2020; accepted 22 January 2021; published 25 February 2021)

Precise knowledge of the charge and rigidity dependence of the secondary cosmic ray fluxes and the secondary-to-primary flux ratios is essential in the understanding of cosmic ray propagation. We report the properties of heavy secondary cosmic ray fluorine F in the rigidity R range 2.15 GV to 2.9 TV based on 0.29 million events collected by the Alpha Magnetic Spectrometer experiment on the International Space Station. The fluorine spectrum deviates from a single power law above 200 GV. The heavier secondary-to-primary F/Si flux ratio rigidity dependence is distinctly different from the lighter B/O (or B/C) rigidity dependence. In particular, above 10 GV, the $\frac{\mathrm{F/Si}}{\mathrm{B/O}}$ ratio can be described by a power law R^{δ} with $\delta = 0.052 \pm 0.007$. This shows that the propagation properties of heavy cosmic rays, from F to Si, are different from those of light cosmic rays, from He to O, and that the secondary cosmic rays have two classes.

DOI: 10.1103/PhysRevLett.126.081102

Fluorine nuclei in cosmic rays are thought to be produced mostly by the collisions of heavy nuclei, such as Ne, Mg, and Si, with the interstellar medium. Together with the much more abundant Li, Be, and B cosmic rays, they are called secondary cosmic rays [1]. Fluorine is the only purely secondary cosmic ray between oxygen and silicon [2]. Fluorine is the heaviest pure secondary cosmic ray accurately measured by AMS.

Over the past 50 years, several experiments have measured the fluorine flux in cosmic rays in kinetic energy per nucleon [3–8] up to 100 GeV/n. The measurement errors exceed 100% at ~50 GeV/n (~100 GV in rigidity). There are no measurements of the F flux in rigidity.

The secondary-to-primary flux ratios of light nuclei in cosmic rays, in particular, B/C or the more direct B/O, have been traditionally used to study the propagation of cosmic rays in the Galaxy [9]. In previous publications, AMS has shown that all light secondary-to-primary ratios, Li/C, Li/O, Be/C, Be/O, B/C, and B/O, deviate from a single power law (harden) above 200 GV [10,11]. This strongly favors that the hardening of all light cosmic rays is due to propagation effects [2,9,12]. Recently, AMS has also studied the properties of the heavy primary Ne, Mg, and Si fluxes [13] and found that they form a separate class of primary cosmic rays. Differences in the rigidity dependence of the F flux and light secondary cosmic ray Li, Be, and B fluxes, as well as differences in the rigidity dependence of light (B/O) and heavy (F/Si) secondary-to-primary flux ratios, provide new important insights on cosmic ray propagation.

In this Letter, we report the precise measurement of the F flux in the rigidity range from 2.15 GV to 2.9 TV based on 0.29 million fluorine nuclei collected by AMS during the first 8.5 years (May 19, 2011 to October 30, 2019) of operation aboard the International Space Station (ISS). The total flux error is 5.9% at 100 GV.

Detector.—The layout and description of the AMS detector are presented in Refs. [11,14] and shown in Fig. S1 of Supplemental Material [15]. The key elements used in this measurement are the permanent magnet [16], the nine layers, $L1$–$L9$, of silicon tracker [17–19], and the four planes of time of flight (TOF) scintillation counters [20]. Further information on the AMS layout, performance, trigger, and the simulations [21,22] is detailed in Supplemental Material [15].

Event selection.—In the first 8.5 years, AMS has collected 1.50×10^{11} cosmic ray events. Fluorine events are required to be downward going and to have a reconstructed track in the inner tracker; see Fig. S2 in Supplemental Material [15] for a reconstructed fluorine event. Details of the event selection are contained in Refs. [23–27] and in Supplemental Material [15].

With this selection, the background from charge-adjacent noninteracting nuclei (O and Ne) due to the finite AMS charge resolution is negligible, $< 0.5\%$ over the whole rigidity range; see Fig. S3 in Supplemental Material [15]. The main background comes from heavier nuclei, such as Ne, Mg, and Si, which interact above tracker $L2$. It has two sources. First, the background resulting from interactions in the material between $L1$ and $L2$ (Transition Radiation Detector and upper TOF) is evaluated by fitting the charge distribution of tracker $L1$ with charge distribution templates of O, F, Ne, and Na. Then cuts are applied on the $L1$ charge as shown in Fig. S4 in Supplemental Material [15]. The charge distribution templates are obtained using $L2$. These templates contain only noninteracting events by requiring that $L1$ and $L3$–$L8$ measure the same charge value. This background varies from 4% to 15% depending on rigidity. Second, the background from interactions in materials above $L1$ (thin support structures made by carbon fiber and aluminum honeycomb) has been estimated from simulation using Monte Carlo samples generated according to AMS flux measurements. The simulation of nuclear interactions has been validated with data using nuclear charge changing cross sections (Ne, Mg, Si, $\ldots \rightarrow \mathrm{F} + X$) [22] measured by AMS, as shown in Fig. S5 in Supplemental Material [15]. This background is estimated to be 14% at 2 GV, 18% at 100 GV, and 15% at 2.9 TV.

After all backgrounds are subtracted, we obtain 0.29×10^6 fluorine nuclei. The uncertainty due to background subtraction is 1.5% at 2 GV, 2% at 100 GV, and 6% at 2.9 TV.

Data analysis.—The isotropic flux Φ_i in the ith rigidity bin $(R_i, R_i + \Delta R_i)$ is given by

$$\Phi_i = \frac{N_i}{A_i \epsilon_i T_i \Delta R_i}, \tag{1}$$

where N_i is the number of events corrected for bin-to-bin migration, A_i is the effective acceptance, ϵ_i is the trigger efficiency, and T_i is the collection time. In this Letter, the flux was measured in 49 bins from 2.15 GV to 2.9 TV, with bin widths chosen according to the rigidity resolution and available statistics.

The bin-to-bin migration of events was corrected using the unfolding procedure described in Ref. [23]. These corrections $(N_i - \aleph_i)/\aleph_i$, where $\aleph_i$ is the number of observed events in bin i, are $+18\%$ at 3 GV, decreasing smoothly to $+5\%$ at 10 GV, -4% at 100 GV, -10% at 300 GV, and -20% at 2.9 TV.

Extensive studies were made of the systematic errors. These errors include the uncertainties in the background evaluation discussed above, the trigger efficiency, the geomagnetic cutoff factor, the acceptance calculation, the rigidity resolution function, and the absolute rigidity scale.

The systematic error on the fluxes associated with the trigger efficiency measurement is $< 1\%$ over the entire rigidity range.

The geomagnetic cutoff factor was varied from 1.0 to 1.4, resulting in a negligible systematic uncertainty ($< 0.1\%$) in the rigidity range below 30 GV.

The effective acceptances A_i were calculated using Monte Carlo simulation and corrected for small differences between the data and simulated events related to (a) event reconstruction and selection, namely, in the efficiencies of velocity vector determination, track finding, charge determination, and tracker quality cuts, and (b) the details of inelastic interactions of nuclei in the AMS materials. The systematic errors on the fluxes associated with the reconstruction and selection are $< 1\%$ over the entire rigidity range.

The material traversed by nuclei from the top of AMS to $L9$ is composed primarily of carbon and aluminum.

The survival probabilities of F nuclei due to interactions in the materials were evaluated using cosmic ray data collected by AMS as described in Ref. [22]. The systematic error due to uncertainties in the evaluation of the inelastic cross section is $< 3\%$ up to 100 GV. Above 100 GV, the small rigidity dependence of the cross section from the Glauber-Gribov model [21] was treated as an uncertainty and added in quadrature to the uncertainties from the measured interaction probabilities [22]. The corresponding systematic error on the F flux is $< 3\%$ up to 100 GV and rises smoothly to 4% at 2.9 TV.

The rigidity resolution function for F has a pronounced Gaussian core characterized by width σ and non-Gaussian tails more than 2.5 σ away from the center [24]. The systematic error on the flux due to the rigidity resolution function was obtained by repeating the unfolding procedure while varying the width of the Gaussian core of the resolution function by 5% and by independently varying the amplitude of the non-Gaussian tails by 10% [24]. The resulting systematic error on the flux is less than 1% below 200 GV and smoothly increasing to 7% at 2.9 TV.

There are two contributions to the systematic uncertainty on the rigidity scale [23]. The first is due to residual tracker misalignment. This error was estimated by comparing the E/p ratio for electrons and positrons, where E is the energy measured with the Electromagnetic Calorimeter and p is the momentum measured with the tracker. It was found to be $1/30$ TV^{-1} [28]. The second systematic error on the rigidity scale arises from the magnetic field map measurement and its temperature corrections. The error on the F flux due to uncertainty on the rigidity scale is $< 1\%$ up to 200 GV and increases smoothly to 6.5% at 2.9 TV.

Most importantly, several independent analyses were performed on the same data sample by different study groups. The results of those analyses are consistent with this Letter.

Results.—The measured F flux including statistical and systematic errors is reported in Table SI in Supplemental Material [15] as a function of the rigidity at the top of the AMS detector. Figure 1(a) shows the F flux as a function of rigidity $\tilde{R}$ with the total errors, the sum in quadrature of statistical and systematic errors. In this and subsequent figures, the data points are placed along the abscissa at $\tilde{R}$ calculated for a flux $\propto R^{-2.7}$ [29]. For comparison, Fig. 1(a) also shows the AMS results on the boron flux [11]. As seen, at high rigidities, the rigidity dependences of the F and B fluxes are identical; at low rigidities, they are different. To examine the rigidity dependence of the F flux, the variation of the flux spectral index γ with rigidity was obtained in a model-independent way from

$$\gamma = d[\log(\Phi)]/d[\log(R)] \tag{2}$$

over nonoverlapping rigidity intervals bounded by 7.09, 12.0, 16.6, 28.8, 45.1, 175.0, and 2900.0 GV. The results are presented in Fig. 1(b) together with the B spectral index [11].

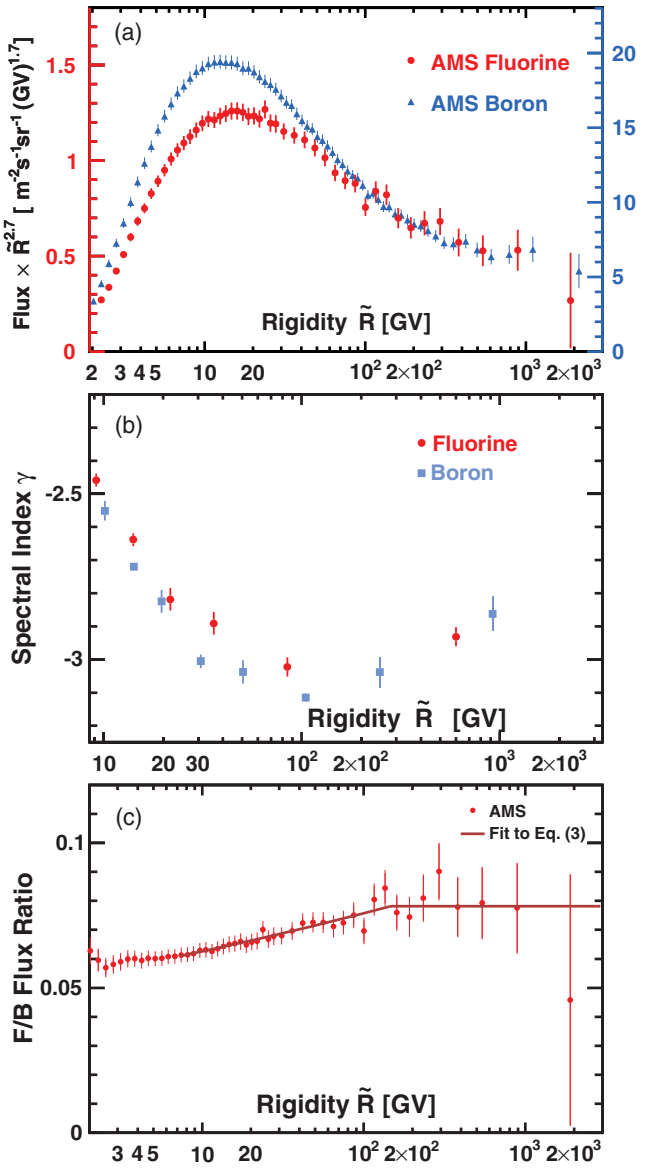

FIG. 1. (a) The AMS fluorine F flux multiplied by $\tilde{R}^{2.7}$ with total errors as a function of rigidity (left axis) together with the AMS boron B flux [11] (right axis). (b) The AMS F spectral index together with the B spectral index [11]. (c) The AMS F/B flux ratio with total errors as a function of rigidity. The brown curve shows the Eq. (3) fit results with $\chi^2/\text{d.o.f.} = 19/33$. As seen, above 150 ± 60 GV, the F/B flux ratio is compatible with a constant.

As seen from Fig. 1(b), in the rigidity interval 175–2900 GV, the F spectral index is similar to the B spectral index. In particular, both fluxes harden above ~200 GV.

To directly compare the rigidity dependence of the F flux with that of the light secondary cosmic ray B flux [11], the ratio of the F flux to the B flux, F/B, was computed and is reported in Table SII in Supplemental Material [15]. To establish the rigidity interval where the F and B fluxes may have identical rigidity dependence, the F/B flux ratio above 7 GV has been fit with

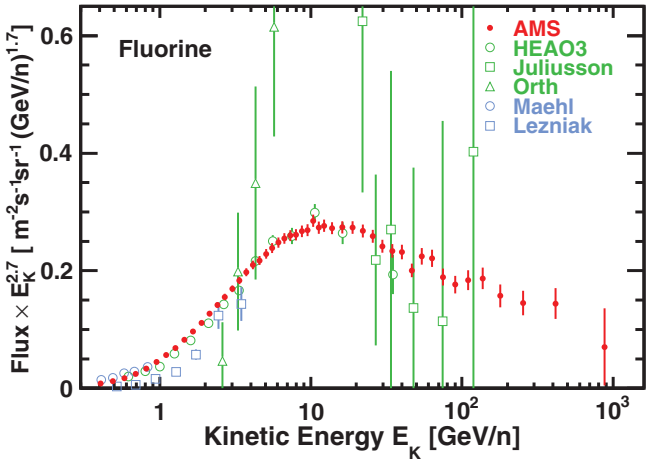

FIG. 2. The AMS fluorine flux as a function of kinetic energy per nucleon E_K multiplied by $E_K^{2.7}$ together with earlier measurements [3–7]. For the AMS measurement, $E_K = (\sqrt{Z^2\tilde{R}^2 + M^2} - M)/A$, where Z, M, and A are the $^{19}_{9}$F nuclear charge, mass, and atomic mass numbers, respectively.

$$\mathrm{F/B} = \begin{cases} \kappa(R/R_0)^{\Delta}, & R \le R_0, \\ \kappa, & R > R_0. \end{cases} \tag{3}$$

The fit yields $\kappa = 0.078 \pm 0.003$, $R_0 = 150 \pm 60$ GV, and $\Delta = 0.083 \pm 0.007$ with $\chi^2/\mathrm{d.o.f.} = 19/33$. Figure 1(c) shows the AMS F/B flux ratio as a function of rigidity with total errors together with the fit results. As seen, above 150 ± 60 GV, the rigidity dependences of the F and B fluxes are identical, and at lower rigidities they are different. As shown in Fig. S6 in Supplemental Material [15], the F/B ratio does not change with time from 5 to 20 GV; i.e., solar modulation of the F/B flux ratio does not affect the fit results with Eq. (3). Note that fitting the F/B ratio with Eq. (3) above 20 GV does not change the fit results. Above 20 GV, the fit yields $\kappa = 0.078 \pm 0.003$, $R_0 = 145 \pm 65$ GV, and $\Delta = 0.084 \pm 0.014$ with $\chi^2/\mathrm{d.o.f.} = 16/21$.

Figure 2 shows the AMS fluorine flux as a function of kinetic energy per nucleon E_K together with earlier measurements [3–7]. Data from other experiments have been extracted using Ref. [30].

To compare the rigidity dependence of the F flux with that of the Ne, Mg, and Si primary cosmic ray fluxes, which have an identical rigidity dependence above 80.5 GV [13], the ratio of the F flux to the characteristic heavy primary Si flux, F/Si, was computed and is reported in Table SIII in Supplemental Material [15]. Figure S7 in Supplemental Material [15] shows the AMS F/Si flux ratio as a function of kinetic energy per nucleon together with earlier measurements [3–7]. Figure 3(a) shows the AMS F/Si flux ratio as a function of rigidity together with the AMS B/O flux ratio [11].

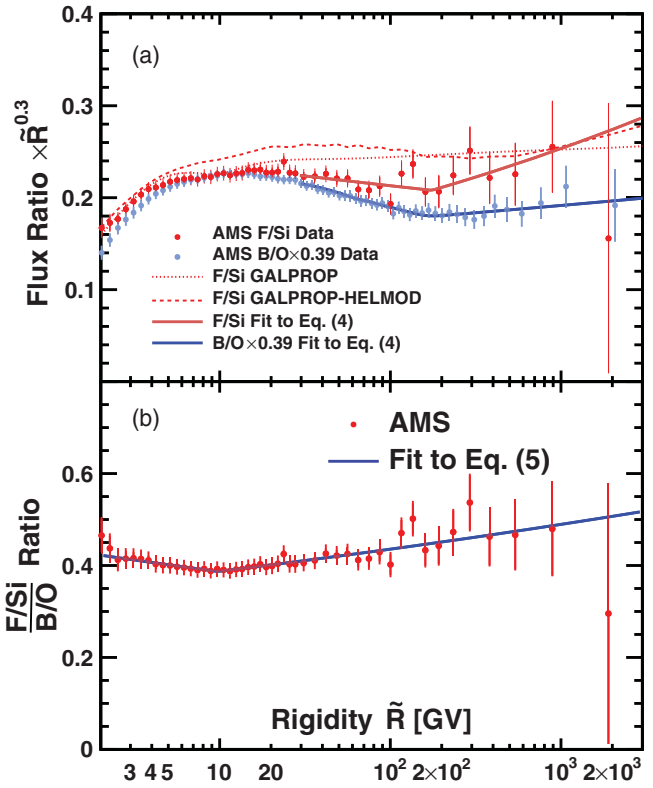

FIG. 3. (a) The AMS F/Si flux ratio (red dots) and AMS B/O flux ratio (blue dots) as a function of rigidity with total errors. For display purposes only, the F/Si and B/O flux ratios are multiplied by $\tilde{R}^{0.3}$ and the B/O flux ratio rescaled as indicated. The solid brown and blue curves show the F/Si and B/O fit results with Eq. (4), respectively. The dotted and dashed red curves show the predictions of the F/Si ratio by the GALPROP model [31] and the GALPROP-HELMOD model [2], respectively. (b) The AMS [(F/Si)/(B/O)] ratio as a function of rigidity with total errors. The solid blue curve shows the fit results of Eq. (5). As seen, the rigidity dependence of the F/Si and B/O flux ratios are distinctly different. Above 10 GV, the [(F/Si)/(B/O)] ratio can be described by a single power law $\propto R^{\delta}$ with $\delta = 0.052 \pm 0.007$ (a 7σ difference from zero).

The variation with rigidity of the spectral index Δ of the F/Si flux ratio was obtained by fitting it with

$$\begin{cases} C(R/175\ \mathrm{GV})^{\Delta_1}, & R \le 175\ \mathrm{GV}, \\ C(R/175\ \mathrm{GV})^{\Delta_2}, & R > 175\ \mathrm{GV}. \end{cases} \tag{4}$$

over the rigidity interval [28.8–2900] GV. The fit yields $C^{\mathrm{F/Si}} = 0.044 \pm 0.001$, $\Delta_1^{\mathrm{F/Si}} = -0.34 \pm 0.02$, and $\Delta_2^{\mathrm{F/Si}} = -0.19 \pm 0.07$ with $\chi^2/\mathrm{d.o.f.} = 13/16$. Above 175 GV, the spectral index $\Delta^{\mathrm{F/Si}}$ exhibits a hardening $(\Delta_2^{\mathrm{F/Si}} - \Delta_1^{\mathrm{F/Si}})$ of 0.15 ± 0.07, compatible with the AMS result on the hardening of the Li/C, Be/C, B/C, Li/O, Be/O, and B/O flux ratios by 0.140 ± 0.025 [10,11]. To ensure that the choice of the inflection point of 175 GV does not affect the fit results, we allowed the inflection point to vary. The results are in complete agreement with results

of Eq. (4); see Supplemental Material [15] for details. Figure 3(a) also shows the AMS F/Si fit results with Eq. (4) together with the predictions of the cosmic ray propagation model GALPROP [31] and of the latest GALPROP-HELMOD model [2] on the F/Si flux ratio and the AMS B/O fit results with Eq. (4), $C^{\mathrm{B/O}} = 0.097 \pm 0.003$, $\Delta_1^{\mathrm{B/O}} = -0.405 \pm 0.005$, and $\Delta_2^{\mathrm{B/O}} = -0.26 \pm 0.03$ with $\chi^2/\mathrm{d.o.f.} = 24/36$.

To compare the rigidity dependence of the F/Si flux ratio with the lighter secondary-to-primary B/O flux ratio in detail, the [(F/Si)/(B/O)] ratio was computed and shown in Fig. 3(b). Over the entire rigidity range, [(F/Si)/(B/O)] can be fitted with

$$\frac{\mathrm{F/Si}}{\mathrm{B/O}} = \begin{cases} k(R/R_0)^{\delta_l}, & R \le R_0, \\ k(R/R_0)^{\delta}, & R > R_0. \end{cases} \quad (5)$$

The fit yields $k = 0.39 \pm 0.01$, $R_0 = 9.8 \pm 0.9$ GV, $\delta_l = -0.055 \pm 0.013$, and $\delta = 0.052 \pm 0.007$ with $\chi^2/\mathrm{d.o.f.} = 24/45$. As seen, the rigidity dependences of the F/Si and B/O flux ratios are distinctly different. Most importantly, the latest AMS result shows that above 10 GV the [(F/Si)/(B/O)] ratio can be described by a single power law $\propto R^{\delta}$ with $\delta = 0.052 \pm 0.007$ (a 7σ difference from zero). This shows, unexpectedly, that the heavier secondary-to-primary F/Si flux ratio rigidity dependence is distinctly different from the lighter B/O (or B/C) rigidity dependence, indicating that the propagation properties of heavy cosmic rays, from F to Si, are different from those of light cosmic rays, from He to O.

As shown in Fig. S8 in Supplemental Material [15], the [(F/Si)/(B/O)] ratio does not change with time below 20 GV; i.e., solar modulation on the [(F/Si)/(B/O)] ratio does not affect the fit results with Eq. (5).

From the results of Eq. (5) and of the Si/O flux ratio rigidity dependence above 86.5 GV [13], we expect $\mathrm{F/B} = [(\mathrm{F/Si})/(\mathrm{B/O})] \times (\mathrm{Si/O}) \propto R^{0.012 \pm 0.013}$ or that F/B is compatible with a constant at high rigidities, > 86.5 GV. This is indeed what is observed, as shown in Fig. 1(c).

Figure 4 shows the rigidity dependence of the F flux together with the rigidity dependence of the two primary classes He, C, and O and Ne, Mg, and Si and the rigidity dependence of the light secondary Li, Be, and B cosmic ray fluxes above 30 GV [11]. As seen, the rigidity dependence of the F flux is different from the rigidity dependence of Li, Be, and B. This shows that the secondary cosmic rays also have two classes but that the rigidity dependence of the two secondary classes is distinctly different from the rigidity dependence of the two primary classes.

In conclusion, we have presented the precision measurement of the F flux as a function of rigidity from 2.15 GV to 2.9 TV, with detailed studies of the systematic errors. The fluorine spectrum deviates from a single power law above 200 GV. The heavier secondary-to-primary F/Si flux ratio rigidity dependence is distinctly different from the lighter B/O (or B/C) rigidity dependence. In particular, above 10 GV, the [(F/Si)/(B/O)] ratio can be described by a power law R^{δ} with $\delta = 0.052 \pm 0.007$, revealing that the propagation properties of heavy cosmic rays, from F to Si, are different from those of light cosmic rays, from He to O. This shows that the secondary cosmic rays also have two classes but that the rigidity dependence of the two secondary classes is distinctly different from the rigidity dependence of the two primary classes. These are new and unexpected properties of cosmic rays.

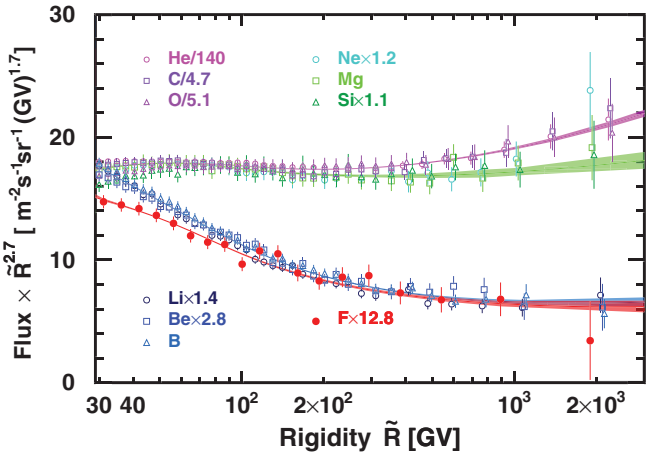

FIG. 4. The rigidity dependence of the F flux compared with the rigidity dependence of the He, C, and O; Ne, Mg, and Si; and Li, Be, and B fluxes above 30 GV. For clarity, the He, O, Ne, Si, Li, and B data points above 400 GV are displaced horizontally. For display purposes only, the He, C, O, Ne, Si, Li, Be, and F fluxes were rescaled as indicated.

We are grateful for important physics discussions with Pasquale Blasi, Fiorenza Donato, Jonathan Feng, and Igor Moskalenko. We thank former NASA Administrator Daniel S. Goldin for his dedication to the legacy of the ISS as a scientific laboratory and his decision for NASA to fly AMS as a DOE payload. We also acknowledge the continuous support of the NASA leadership, particularly William H. Gerstenmaier, and of the Johnson Space Center (JSC) and Marshall Space Flight Center (MSFC) flight control teams that have allowed AMS to operate optimally on the ISS for over nine years. We are grateful for the support of Jim Siegrist, Glen Crawford, and their staff of the DOE including resources from the National Energy Research Scientific Computing Center under Contract No. DE-AC02-05CH11231. We gratefully acknowledge the strong support from CERN including Fabiola Gianotti, and the CERN IT department including Bernd Panzer-Steindel, and from the European Space Agency including Johann-Dietrich Wörner and Simonetta Di Pippo. We also acknowledge the continuous support from MIT and its School of Science, Michael Sipser, and the Laboratory for Nuclear Science, Boleslaw Wyslouch. Research supported by Chinese Academy of Sciences, Institute of High Energy

Physics, Institute of Electrical Engineering, China Academy of Space Technology, National Natural Science Foundation, and Ministry of Science and Technology, the China Scholarship Council, the provincial governments of Shandong, Jiangsu, Guangdong, Shandong University, and the Shandong Institute of Advanced Technology, China; the Academy of Finland, Project No. 321882, Finland; CNRS/IN2P3 and CNES, France; DLR under Grants No. 50OO1403 and No. 50OO1805 and computing support on the JARA Partition of the RWTH Aachen supercomputer, Germany; INFN and ASI under ASI-INFN Agreements No. 2014-037-R.1-2017 and No. 2019-19-HH.0 and ASI-University of Perugia Agreement No. 2019-2-HH.0, Italy; CHEP and NRF under Grant No. NRF-2018R1A6A1A06024970 at Kyungpook National University, Korea; the Consejo Nacional de Ciencia y Tecnología and UNAM, Mexico; NWO under Grant No. 680-1-004, Netherlands; FCT under Grant No. CERN/FIS-PAR/0013/2019, Portugal; the Ministry of Science and Higher Education under Project No. 0723-2020-0040, Russia; CIEMAT, IAC, CDTI, and SEIDI-MINECO under Grants No. PID2019–107988 GB-C21/C22, No. CEX2019-000920-S, and No. MDM-2015-0509, Spain; the Swiss National Science Foundation (SNSF), federal and cantonal authorities, and the Fondation Dr. Manfred Steuer, Switzerland; Academia Sinica and the Ministry of Science and Technology (MOST) under Grants No. 107-2119-M-006-015-MY3, No. 109-2112-M-001-029, and No. CDA-105-M06, former Presidents of Academia Sinica Yuan-Tseh Lee and Chi-Huey Wong and former Ministers of MOST Maw-Kuen Wu and Luo-Chuan Lee, Taiwan; the Turkish Energy, Nuclear and Mineral Research Agency (TENMAK) under Grant No. 2020TAEK(CERN)A5.H1.F5-26, Turkey; and NSF Grants No. 1455202 and No. 1551980, Wyle Laboratories Grant No. 2014/T72497, and NASA NESSF Grant No. HELIO15F-0005, USA.

[*]Also at Nikhef, 1098 XG Amsterdam, Netherlands.
[†]Also at ASI Space Science Data Center (SSDC), 00133 Roma, Italy.
[‡]Also at Policlinico S. Orsola-Malpighi, 40138 Bologna, Italy.

[1] I. A. Grenier, J. H. Black, and A. W. Strong, Annu. Rev. Astron. Astrophys. **53**, 199 (2015); P. Blasi, Astron. Astrophys. Rev. **21**, 70 (2013); A. W. Strong, I. V. Moskalenko, and V. S. Ptuskin, Annu. Rev. Nucl. Part. Sci. **57**, 285 (2007); A. Castellina and F. Donato, Astropart. Phys. **24**, 146 (2005).
[2] M. J. Boschini *et al.*, Astrophys. J. Suppl. Ser. **250**, 27 (2020).
[3] E. Juliusson, Astrophys. J. **191**, 331 (1974).
[4] R. Maehl, J. F. Ormes, A. J. Fisher, and F. A. Hagen, Astrophys. Space Sci. **47**, 163 (1977).
[5] C. D. Orth, A. Buffington, G. F. Smoot, and T. S. Mast, Astrophys. J. **226**, 1147 (1978).
[6] J. Lezniak and W. Webber, Astrophys. J. **223**, 676 (1978).
[7] J. J. Engelmann *et al.*, Astron. Astrophys. **233**, 96 (1990).
[8] K. Lave *et al.*, Astrophys. J. **770**, 117 (2013).
[9] C. Evoli, R. Aloisio, and P. Blasi, Phys. Rev. D **99**, 103023 (2019). As stated in this paper, the O flux has much less of a secondary component than the C flux, so the B/O flux ratio is a better indicator of the material grammage traversed by cosmic rays.
[10] M. Aguilar *et al.*, Phys. Rev. Lett. **120**, 021101 (2018).
[11] M. Aguilar *et al.*, Phys. Rep. **894**, 1 (2021); the comprehensive paper on results for elements F, Na, and Al, which includes details of the analysis, particularly at high energies, and comparison with theoretical models, will be submitted to Phys. Rev. D.
[12] N. Weinrich, Y. Génolini, M. Boudaud, L. Derome, and D. Maurin, Astron. Astrophys. **639**, A131 (2020).
[13] M. Aguilar *et al.*, Phys. Rev. Lett. **124**, 211102 (2020).
[14] A. Kounine, Int. J. Mod. Phys. E **21**, 1230005 (2012); S. Rosier-Lees, in *Proceedings of Astroparticle Physics TEVPA/IDM, Amsterdam, 2014* (unpublished); S. Ting, Nucl. Phys. B, Proc. Suppl. **243–244**, 12 (2013); S.-C. Lee, in *Proceedings of the 20th International Conference on Supersymmetry and Unification of Fundamental Interactions (SUSY 2012), Beijing, 2012* (unpublished); M. Aguilar, in *Proceedings of the XL International Meeting on Fundamental Physics, Centro de Ciencias de Benasque Pedro Pascual, 2012* (unpublished); S. Schael, in *Proceedings of the 10th Symposium on Sources and Detection of Dark Matter and Dark Energy in the Universe, Los Angeles, 2012* (unpublished); B. Bertucci, *Proc. Sci.*, EPS-HEP2011 (2011) 067; M. Incagli, AIP Conf. Proc. **1223**, 43 (2010); R. Battiston, Nucl. Instrum. Methods Phys. Res., Sect. A **588**, 227 (2008).
[15] See Supplemental Material at http://link.aps.org/supplemental/10.1103/PhysRevLett.126.081102 for the AMS detector description, details of event selection, the tabulated F flux, and the F/Si and F/B flux ratios all as functions of rigidity; and figures regarding the detector, charge selection, systematic errors, and the AMS F/Si flux ratio as a function of kinetic energy together with earlier measurements.
[16] K. Lübelsmeyer *et al.*, Nucl. Instrum. Methods Phys. Res., Sect. A **654**, 639 (2011).
[17] B. Alpat *et al.*, Nucl. Instrum. Methods Phys. Res., Sect. A **613**, 207 (2010).
[18] Y. Jia, Q. Yan, V. Choutko, H. Liu, and A. Oliva, Nucl. Instrum. Methods Phys. Res., Sect. A **972**, 164169 (2020).
[19] G. Ambrosi, V. Choutko, C. Delgado, A. Oliva, Q. Yan, and Y. Li, Nucl. Instrum. Methods Phys. Res., Sect. A **869**, 29 (2017).
[20] V. Bindi *et al.*, Nucl. Instrum. Methods Phys. Res., Sect. A **743**, 22 (2014).
[21] J. Allison *et al.*, Nucl. Instrum. Methods Phys. Res., Sect. A **835**, 186 (2016); IEEE Trans. Nucl. Sci. **53**, 270 (2006); S. Agostinelli *et al.*, Nucl. Instrum. Methods Phys. Res., Sect. A **506**, 250 (2003).
[22] Q. Yan, V. Choutko, A. Oliva, and M. Paniccia, Nucl. Phys. **A996**, 121712 (2020).

[23] M. Aguilar *et al.*, Phys. Rev. Lett. **114**, 171103 (2015).
[24] M. Aguilar *et al.*, Phys. Rev. Lett. **115**, 211101 (2015).
[25] M. Aguilar *et al.*, Phys. Rev. Lett. **117**, 231102 (2016).
[26] J. Alcaraz *et al.*, Phys. Lett. B **484**, 10 (2000).
[27] C. C. Finlay *et al.*, Geophys. J. Int. **183**, 1216 (2010); E. Thébault *et al.*, Earth Planets Space **67**, 79 (2015); Geomagnetic Field Modeling Working Group, *IGRF-13 Model* (2019), https://www.ngdc.noaa.gov/IAGA/vmod/igrf.html.
[28] J. Berdugo, V. Choutko, C. Delgado, and Q. Yan, Nucl. Instrum. Methods Phys. Res., Sect. A **869**, 10 (2017).
[29] G. D. Lafferty and T. R. Wyatt, Nucl. Instrum. Methods Phys. Res., Sect. A **355**, 541 (1995). We have used Eq. (6) with $\tilde{R} \equiv x_{lw}$.
[30] D. Maurin, F. Melot, and R. Taillet, Astron. Astrophys. **569**, A32 (2014).
[31] We used GALPROP WebRun, A. E. Vladimirov, S. W. Digela, G. Jóhannesson, P. F. Michelson, I. V. Moskalenko, P. L. Nolan, E. Orlando, T. A. Porter, and A. W. Strong, Comput. Phys. Commun. **182**, 1156 (2011); with parametrization from R. Trotta, G. Jóhannesson, I. V. Moskalenko, T. A. Porter, R. Ruiz de Austri, and A. W. Strong, Astrophys. J. **729**, 106 (2011).